Energy Storage Materials 21 (2019) 50–60

Contents lists available at ScienceDirect

Energy Storage Materials

journal homepage: www.elsevier.com/locate/ensm

Let thermodynamics do the interfacial engineering of batteries and solid electrolytes

Jian Luo

Department of NanoEngineering, Program of Materials Science and Engineering, University of California, San Diego, 9500 Gilman Drive, La Jolla, CA, 92093-0448, USA

ARTICLE INFO

Keywords:
2D interfacial phase
Complexion
Interfacial engineering
Solid electrolyte
Solid-state battery

ABSTRACT

This review/perspective article critically assesses recent efforts and emerging opportunities to utilize the equilibrium formation of 2D interfacial phases to tailor batteries and solid electrolytes. In contrast to traditional kinetically-controlled atomic layer deposition (ALD) and other interfacial engineering methods, these 2D interfacial phases form spontaneously at thermodynamic equilibria; they are also termed as "complexions" to differentiate them from thin layers of 3D bulk phases whose thicknesses are controlled by kinetic/processing parameters such as the number of ALD cycles or deposition time. Here, two classic examples are represented by the impurity (dopant) based surface amorphous films (SAFs) and intergranular films (IGFs), both of which possess thermodynamically-determined "equilibrium" thicknesses on the order of 1 nm. Recently, the spontaneous formation of nanometer-thick SAFs and other less-disordered 2D surface phases have been utilized to improve the rate capability and cycling stability of various electrode materials. Detrimental and beneficial IGFs and other prewetting-like 2D interfacial phases have also been found in solid electrolytes or the solid electrolyte-electrode interfaces. A variety of other complexions, e.g., ordered adsorbates, can also play important, yet unrecognized, roles in various battery systems and solid electrolytes. Opportunities of utilizing 2D interfacial phases to control or improve the processing, ionic conductivity, and interfacial stability in solid electrolytes as well as solid-state and other battery systems are discussed. A potentially transformative idea is to utilize 2D interfacial phases to achieve superior properties unattainable by conventional bulk phases since they can exhibit structures that are neither observed nor necessarily stable as 3D bulk phases.

1. Introduction

Various kinetically-controlled methods, such as the atomic layer deposition (ALD), have been used to tailor the battery interfaces successfully [1–17]; yet, there are limitations, e.g., the scalability and cost of ALD. This review critically assesses an emerging opportunity of using equilibrium formation of 2D interfacial phases (also known as "complexions" [18–21]), which form spontaneously as thermodynamic equilibria, as a new and innovative method to engineer battery interfaces. In other words, let thermodynamics tailor the interfaces for us.

For example, spontaneous formation of dopant-based 2D surface phases via facile "mixing and annealing" have been utilized to improve the rate capability and cycling stability of various cathode and anode materials [22–28]. Here, a class of surface amorphous films (SAFs) with self-selecting or "equilibrium" thicknesses have been systematically characterized [22–25,29,30]; other types of surface adsorbates may also form to enhance the battery performance [26,27]. These nanoscale SAFs were originally discovered as the free-surface counterparts to the intergranular (glassy) films (IGFs) that are well-known in the ceramic community since 1980s [31,32]. Recently studies also found equilibrium-thickness IGFs and other similar complexions at the grain boundaries in solid electrolytes and solid electrolyte-electrode interfaces, which can have detrimental or beneficial effects to solid-state batteries or other energy devices [33–38]. Furthermore, other ordered 2D interfacial phases can also exist and play important, yet unrecognized, roles in various battery systems, including metallic anodes and solid electrolyte-electrode interfaces that have been less well characterized to date.

Moreover, several reports showed significantly enhanced ionic conductivities in SAFs and IGFs [33–36]. This further supports a potentially transformative idea of utilizing 2D interfacial phases to achieve superior properties unattainable by 3D bulk phases. This is possible in part because these 2D interfacial phases can exhibit structures and/or compositions that are neither observed nor necessarily stable as 3D bulk phases, e.g., structures that are between a glass and a crystal (despite the historical names of "amorphous" SAFs or "glassy" IGFs) and average

E-mail address: jluo@alum.mit.edu.

https://doi.org/10.1016/j.ensm.2019.06.018
Received 13 April 2019; Received in revised form 9 June 2019; Accepted 14 June 2019
Available online 21 June 2019

compositions that lie within the bulk miscibility gaps [19,20,29,32,36]. Emerging opportunities for utilizing such 2D interfacial phases or complexions to control and improve the processing and properties of solid electrolytes and solid-state and other battery systems are discussed.

2. Equilibrium formation of SAFs: let thermodynamics make nanoscale coatings

It is now well-established that nanoscale surface oxide coatings made by ALD can improve the cycling stability and other performance properties of electrode materials in both conventional and solid-state batteries [1–17]. While uniform nanoscale coatings can be fabricated with atomic level controls, ALD requires special equipment and chemicals that limit its scalability and add cost. Recent studies have established an alternative strategy through a facile "mixing and annealing" route to spontaneously form nanometer-thick SAFs at thermodynamic equilibria [22–25,29,30].

Luo et al. originally discovered dopant-based SAFs as a new class of 2D surface phases, which are characterized by the following distinct traits [23,24,29,39–43].

(1) they possess self-selecting or "equilibrium" thicknesses on the order of 1 nm that are tunable by changing the equilibrium temperature or chemical potential;
(2) they have been named as surface "amorphous" films or SAFs (historically) despite that their structures are neither fully amorphous nor completely crystalline (distinct from any bulk glass or crystal);
(3) they exhibit intrinsic through-thickness structural and compositional gradients;
(4) they have average compositions that differ from the associated bulk phases (*e.g.*, even within the bulk immiscible region that would be unstable as a bulk phase); and
(5) they show thermodynamic stabilities that markedly differ from the associated bulk phases (*e.g.*, quasi-liquid SAFs can form well below the bulk solidus temperature, where the bulk liquid phase is not stable thermodynamically).

Because of some of the above unique characters of the SAFs, a potentially-transformative opportunity is envisioned to utilize such spontaneously-formed 2D surface phases to achieve properties unattainable by 3D bulk phases.

We can form such SAFs via (1) mixing of the powder of our primary material with a small amount of a surface-active additive (high-temperature adsorbates, e.g., V_2O_5 for the TiO_2 powder as discussed below) via either dry mixing (by ball milling of two powders directly) or a wet route (by adding a solution of a salt that contains the needed metal cations, which will decompose in the subsequent annealing step, e.g., a NH_4VO_3 + NH_4OH solution for forming V_2O_5 based SAFs after annealing), followed by (2) isothermal annealing at a desired temperature to allow the particle surfaces to achieve their thermodynamic equilibrium state, which is represented by nanoscale SAFs of an "equilibrium" thickness. This facile "mixing and annealing" process is simpler than most thin-film deposition procedures (such as ALD), it does not require special thin-film deposition equipment, and it can be scaled up easily to a very-large-scale production.

As an example, Fig. 1(a) shows a V_2O_5-based SAF formed spontaneously on the surface of TiO_2 upon a facile "mixing and annealing" process [29,44]. These SAFs process thermodynamically-determined "equilibrium" thickness that is independent of kinetic factors (Fig. 1(b)); but this

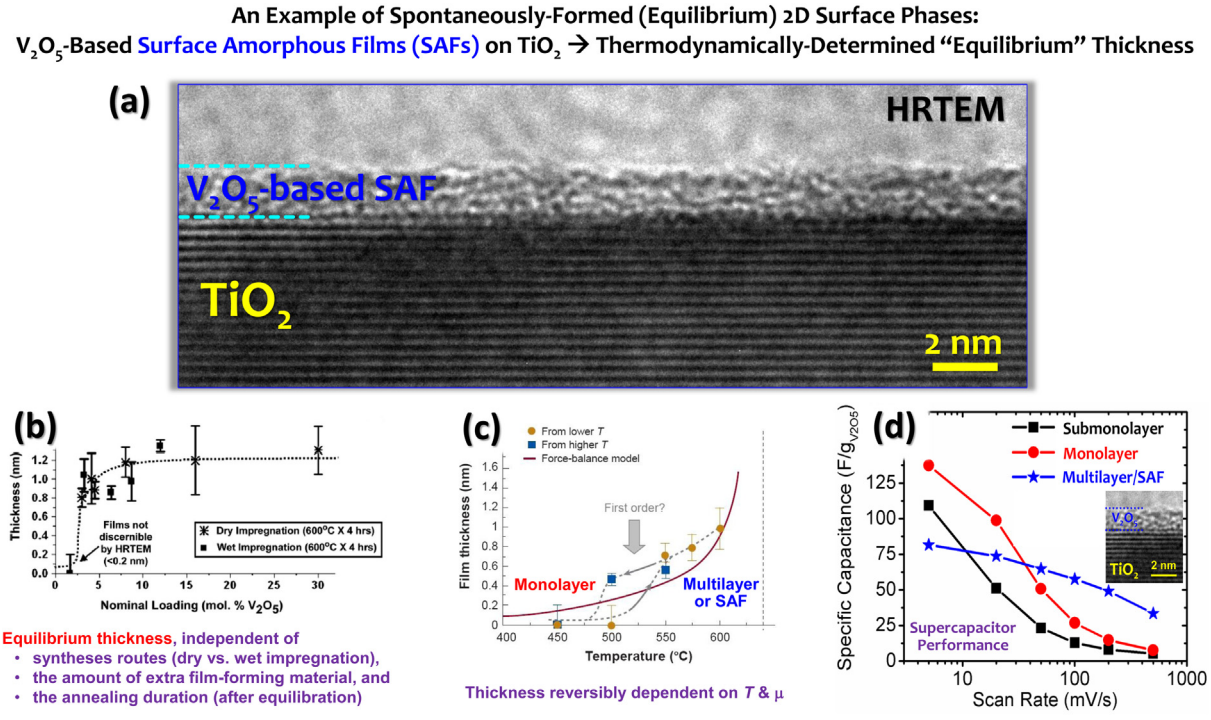

Fig. 1. An example of equilibrium 2D interfacial phases (complexions): V_2O_5-based surface amorphous films (SAFs) on TiO_2 with a self-selecting or "equilibrium" thickness. **(a)** A representative high-resolution transmission electron microscopy (HRTEM) image of a nanometer-thick V_2O_5-based SAF formed spontaneously on TiO_2 (at a thermodynamic equilibrium) upon facile "mixing and annealing." **(b)** These spontaneously-formed SAFs adopt a thermodynamically-determined (equilibrium) thickness that is independent of kinetic factors (*e.g.*, the synthesis routes, the annealing time, and excess amount of film-forming species as shown here) after reaching a thermodynamic equilibrium [29,44]. **(c)** Yet, this equilibrium thickness reversibly depends on thermodynamic potentials, such as the equilibrium temperature (or the chemical potential of another co-dopant [45]); furthermore, the hysteresis loop indicates the existence of a first-order phase-like transformation [44]. **(d)** The nanoscale SAFs (i.e., multilayer adsorbates) surprisingly exhibit improved pseudocapacitive capacitances at high scan rates in comparison with the monolayer surface adsorbates, which is presumed due to the partial order and excess free volume in the nanoscale amorphous-like SAFs [129]. This figure is replotted by adapting and combining original figures reported in Refs. [44,129] with permission.

equilibrium thickness depends on (thereby being tunable by changing) thermodynamic potentials, such as temperature (Fig. 1(c)) [44] or chemical potential (not shown here, but being demonstrated in a separate study [45]). Moreover, Fig. 1(c) shows a reversible temperature-dependence of the equilibrium thickness, where the hysteresis loop indicates a first-order surface phase-like transformation [44]. Interestingly, these nanometer-thick SAFs (a.k.a. multilayer V_2O_5-based adsorbates) exhibit improved pseudocapacitive capacitances (per gram of the active material) at high scanning rates in comparison with the monolayer surface adsorbates (Fig. 1(d)); this counterintuitive observation is likely a result of the partial order and excess free volume in the amorphous-like surface phases. This surprising observation (Fig. 1(d)) supports the hypothesized possibility of achieving unique properties via the partially-ordered and partially-disordered structures in 2D interfacial phases that differ significantly from any 3D bulk phases.

A thermodynamic model [29,46] for the SAFs is briefly discussed here. In this phenomenological interfacial thermodynamic model, we treat an SAF as a quasi-liquid film with modified structure (*e.g.*, partial order) and thermodynamic properties. First, a quasi-liquid film will spontaneously coat on (i.e. completely wet) the surface of the crystalline electrode if replacing a crystal-vapor surface ($\gamma_{cv}^{(0)}$) with the liquid-vapor ($\gamma_{\rm lv}$) and crystal-liquid ($\gamma_{\rm cl}$) interfaces lowers the free energy:

$$\gamma_{\rm cl} + \gamma_{\rm lv} < \gamma_{cv}^{(0)}, \tag{1}$$

Here, the superscript "(0)" in $\gamma_{cv}^{(0)}$ denotes a "clean" surface with no adsorption of the liquid specie (dopant). Eq. (1) suggests us to select an SAF-forming or "coating" material with a lower surface energy. It also implies that an SAF should generally prefer to be structurally disordered to avoid a high crystal-crystal interfacial energy (unless a coherent interface can form).

Second, a quasi-liquid SAF of thickness h can be thermodynamically stabilized below the bulk solidus curve, where the bulk liquid phase is no longer stable, if:

$$-\Delta\gamma \equiv \gamma_{cv}^{(0)} - (\gamma_{cl} + \gamma_{lv}) > \Delta G_{\rm amorph}^{(\rm vol)} \cdot h\,, \tag{2}$$

where $\Delta G_{\rm amorph}^{(\rm vol)}$ is the volumetric free-energy penalty for amorphization or forming an undercooled liquid (Fig. 2(a)).

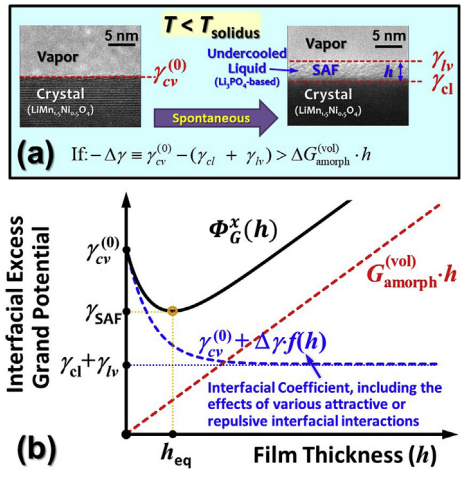

Fig. 2. **(a)** Schematic illustration of the thermodynamic principle for stabilizing a nanometer-thick SAF below the bulk solidus line, using Li_3PO_4-based SAFs formed spontaneously on $LiNi_{0.5}Mn_{1.5}O_4$ as an example [24]. **(b)** Schematic illustration of the interfacial excess grand potential *vs.* film thickness curve for the formation an SAF well below the bulk solidus curve, where the volumetric free energy penalty for forming an undercooled quasi-liquid SAF of thickness h is the dominant attractive interaction. The equilibrium thickness ($h_{\rm eq}$) corresponds to the minimum in $\Phi_G^x(h)$. This figure is adapted from Ref. [24] with permission.

Third, the underneath crystal can often impose significant partial structural order into the SAF when its thickness is on the order of 1 nm [29,47]. Thus, these SAFs are not fully liquid/amorphous, despite that they were named as surface "amorphous" films [29]. Interestingly, such partial structural order may promote ion transport to achieve high rate capabilities for pseudocapacitors shown in Fig. 1(d); moreover, it may enable an interfacial ionic conductivity that is higher than those of both the bulk crystal and glass (to be discussed further in §5) [48,49].

Moreover, additional interfacial interactions should arise when the film thickness is in the nanometer range. Thus, the excess interfacial grand potential can be written as:

$$\Phi_G^x(h) = (\gamma_{cl} + \gamma_{lv}) + \Delta G_{\rm amorph}^{(\rm vol)} \cdot h + \sigma_{\rm short-range}(h) + \sigma_{\rm vdW}(h) + \sigma_{\rm elec}(h) + \ldots, \tag{3}$$

which include short-range, van der Waals (vdW) London dispersion, electrostatic interactions (written as independent terms for simplicity). The SAF will adopt an "equilibrium" thickness ($h_{\rm eq}$) that minimizes the interfacial excess grand potential ($d\Phi_G^x/dh|_{h\,=\,h{\rm eq}} = 0$, Fig. 1(b)). This can be equivalently considered as a balance among attractive or repulsive pressures (derivatives of the interfacial interaction terms in Eq. (3)) acting on the film following the Clarke model [29,31,41,50,51]. At a thermodynamic equilibrium, the two interfaces are no longer independent and become one crystal-vapor surface thermodynamically [52], where equilibrium surface energy corresponds to the minimum of the interfacial excess grand potential expressed in Eq. (3):

$$\gamma_{cv}^{(eq)} = \gamma_{\rm SAF} = \min\{\Phi_G^x(h)\} = \Phi_G^x(h_{\rm eq}) \le \gamma_{cv}^{(0)} \equiv \Phi_G^x(0). \tag{4}$$

Quantifying all interfacial interactions in Eq. (3) is infeasible, but we can define a dimensionless interfacial coefficient, $f(h) \equiv \Sigma_i\sigma_i(h)]/\Delta\gamma + 1$, to simplify Eq. (3) to:

$$\Phi_G^x(h) - \gamma_{cv}^{(0)} = \Delta\gamma \cdot f(h) + \Delta G_{\rm amorph}^{(\rm vol)} \cdot h, \tag{5}$$

Then, Eq. (2) can be refined to a more rigorous inequality:

$$-\Delta\gamma \cdot f(h_{\rm eq}) > \Delta G_{amorph}^{(vol)} \cdot h_{\rm eq}. \tag{6}$$

The boundary conditions require that: $f(0) = 0$ and $f(+\infty) = 1$ (though $f(h)$ is not necessarily monotonic). A sketch of $\Phi_G^x(h)$ for the stabilization of a quasi-liquid SAF well below the bulk solidus curve is shown in Fig. 2(b).

Inspired by an original study of Kang and Ceder [22], a series of studies [22,24,25,28,34,53–56] suggested that the spontaneous formation of phosphate-based SAFs upon mixing and annealing can improve the rate capability and cycling stability of Li-ion battery materials. Several examples (i.e., Li_3PO_4-based SAFs on $LiNi_{0.5}Mn_{1.5}O_4$ [24], $LiCoO_2$ [24], and $Li_{1.33}Ni_{0.3}Mn_{0.57}O_4$ [25]) are shown in Fig. 3(a)-(c), and they will be further discussed in §4.

3. A broad perspective: IGFs, Gibbs adsorption, prewetting, premelting, and complexion

We shall further discuss a spectrum of related interfacial phenomena, as follows. First, SAFs were discovered as the free-surface counterparts to the impurity-based intergranular films or IGFs that have been widely observed at grain and solid-solid phase boundaries in various structural and functional ceramics [31,32,50]. Fig. 4(a) shows the simultaneous formation of nanometer-thick SAFs and an IGF with similar character in a battery system. Clarke initially proposed that these IGFs adopt a nanoscale "equilibrium" thickness [31,50]. The metallic counterparts to these ceramic IGFs have also been observed [57–61], thereby demonstrating the wide-spreading existence of similar 2D interfacial phases.

Second, Cannon et al. [62] suggested that these impurity-based IGFs (and the analogous SAFs) can be alternatively and equivalently interpreted as a special class of structurally-disordered multilayer adsorbates,

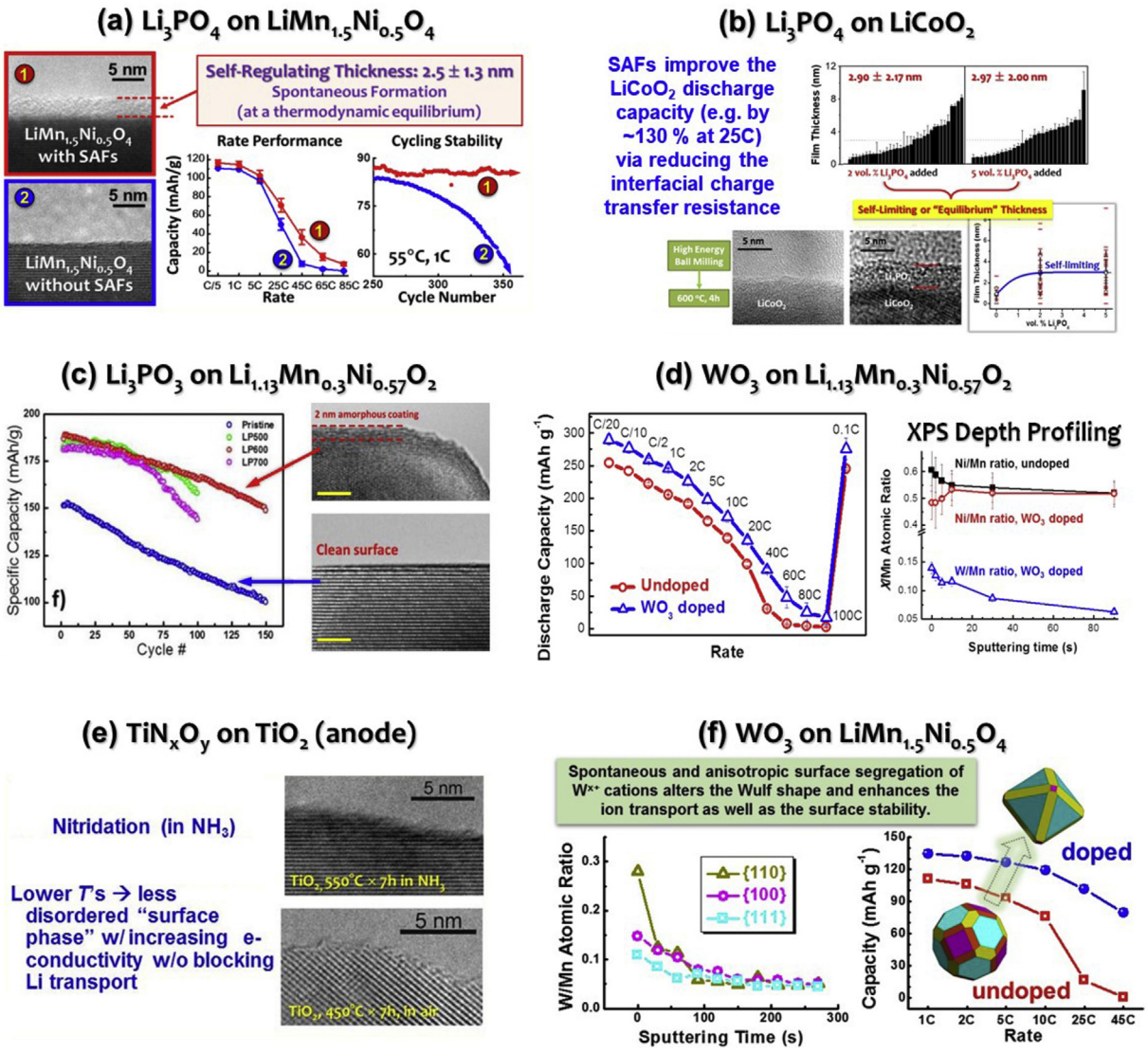

Fig. 3. Six examples of utilizing spontaneously-formed 2D surface phases to improve Li-ion batteries. Spontaneous formation of nanometer-thick Li_3PO_4-based SAFs on **(a)** $LiNi_{0.5}Mn_{1.5}O_4$ [24], **(b)** $LiCoO_2$ [24], and **(c)** $Li_{1.33}Ni_{0.3}Mn_{0.57}O_4$ [25] at thermodynamic equilibria upon facile "mixing and annealing" can increase the rate capabilities (by reducing the interfacial charge transfer resistance) and cycling stability (by suppressing the SEI growth) of these cathode materials. In panel (c), LP500, LP600 and LP700 represent specimens with SAFs formed (equilibrated) at 500 °C, 600 °C, and 700 °C, respectively. **(d)** The formation of a WO_3-rich surface phase on $Li_{1.33}Ni_{0.3}Mn_{0.57}O_4$, which decreases the surface Ni/Mn ratio and changes the surface valence state, can improve the discharge capacities at all rates [27]. **(e)** Surface nitridation of the TiO_2 anode materials can lead to the formation of a TiO_xN_y-based 2D surface phase to increase the rate capability by increasing the surface electronic conductivity [26]. **(f)** Formation of WO_3-rich 2D surface phases on $LiNi_{0.5}Mn_{1.5}O_4$ can change the Wulff shape of the cathode particles via anisotropic segregation of tungsten, which can subsequently increase the rate capability by increasing the fraction of fast-charging {110} facets [30]. This figure is replotted by adapting and combining original figures in Refs. [24–27,30] with permission.

where the Gibbs adsorption theory should rigorously hold.

Third, the stabilization of impurity-based, quasi-liquid SAFs and IGFs below the bulk solidus curve is analogous to the well-known phenomenon of "premelting" in unary systems [63–65] as well as the "prewetting" in Cahn's critical point wetting model [41,66,67]. In its general definition, prewetting refers to the thermodynamic stabilization of a thin β-like layer at an interface due to the reduction in the interfacial energy when the bulk β phase is not yet stable. In this regard, premelting, also known as "surface melting," can be considered as a special case of prewetting in a one-component solid-liquid-vapor system, where a quasi-liquid layer is stabilized at the solid-vapor interface below the melting temperature in the same unary system.

At a more fundamental level, both physicists and materials scientists have long recognized that interfaces can exhibit phase-like transformations. While the term "surface phase" is commonly used by the physics community, Hart first proposed in 1968 to treat grain boundaries as 2D interfacial phases [68,69]. Subsequently, Hondros and Seah [70,71], Cahn [66,72–74], Clarke [31,50], Carter et al. [18,20,67,75,76], Wynblatt and Chatain [77–79], Mishin et al. [80–84], and Luo et al. [85–88] developed relevant thermodynamic models to further elaborate this concept. Tang, Carter, and Cannon [18,67] named such 2D interfacial phases as "complexions," to differentiate them from thin layers of 3D bulk phases precipitated at interfaces.

Specifically, a series of discrete complexions has been observed in Al_2O_3 by Dillon and Harmer (Fig. 5(a)) [21,89–91], and subsequently in other ceramic and metallic materials [58,60,92–97]. These Dillon-Harmer complexions can be considered as derivatives to IGFs with discrete (yet nominal) thicknesses of 0, 1, 2, 3, x, and $+\infty$ atomic layers (Fig. 5(a)). The fundamental aspects of complexions and related interfacial phenomena were recently reviewed [19,20]. We expect other complexions (a.k.a. 2D interfacial phases) beyond nanoscale SAFs and IGFs may also play important, yet largely unrecognized, roles in batteries

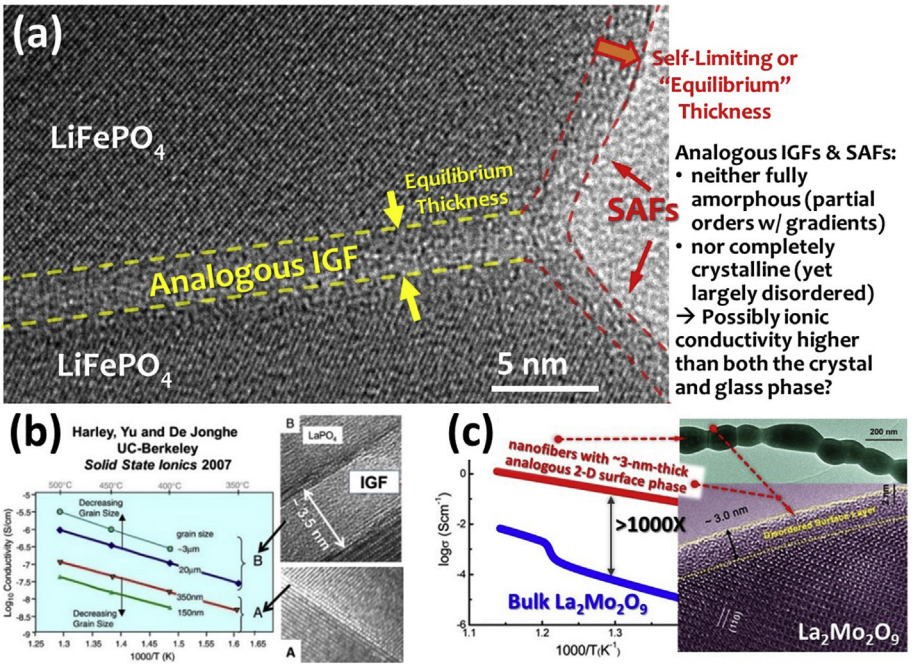

Fig. 4. Examples of promoting ionic transport with nanometer-thick 2D interfacial phases. **(a)** Phosphate-based, nanometer-thick SAFs and their grain-boundary counterparts, intergranular films (IGFs), can form in annealed battery cathode particles to provide a fast Li^+ conduction pathway [22,28,34]. This HRTEM micrograph also illustrate the simultaneous formation of analogous nanoscale SAFs and an IGF of similar character. **(b)** The formation of 1–4 nm thick phosphate-based IGFs in $LaPO_4$ can increase its proton conductivities by > 10X [35]. **(c)** The formation of ~3-nm-thick SAFs, curved on nanofibers, can enhance the oxygen conductivities of $La_2Mo_2O_9$ nanowires by > 1000X [33]. This figure is replotted by adapting and combining original figures reported in Refs. [33–35] with permission.

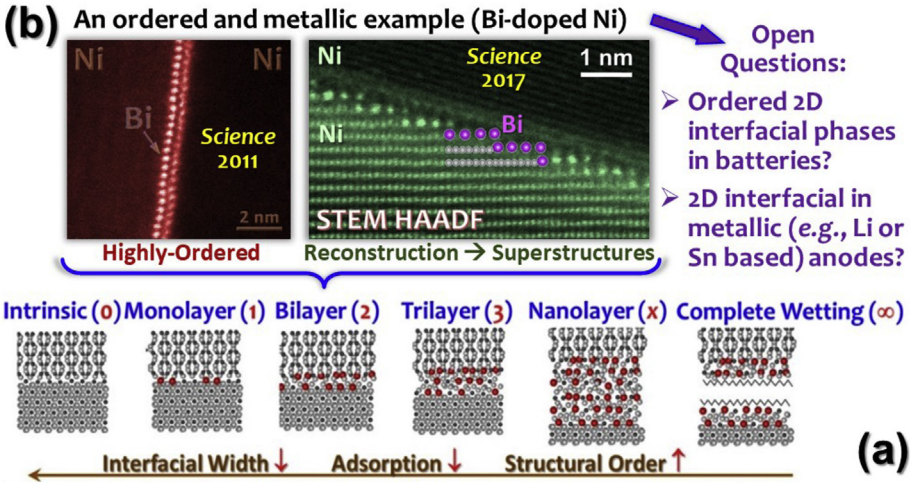

Fig. 5. (a) Schematic illustration of a series of 2D interfacial phases (Dillon-Harmer complexions [19,21,90]), which may be considered as discrete IGFs with nominal thickness of 0, 1, 2, 3, x, and $+\infty$ monolayer(s) [19,86,130]. **(b)** One example is represented by the highly-ordered bismuth (Bi) adsorbates at nickel (Ni) general grain boundaries [96] with interfacial reconstructions [97]. This figure is replotted by adapting and combining original figures reported in Refs. [96,97] with permission. The recent observations [96,97] of thinner and significantly more ordered 2D interfacial phases in metallic model systems (than the SAFs/IGFs observed previously in oxide battery materials) call for further investigation of the following open questions: (1) Can similar ordered 2D adsorbates exist and play important roles in controlling battery interfaces? (2) What are the characteristics of the 2D interfacial phases in metallic electrodes, such as lithium (Li) or tin (Sn) anodes?

and solid electrolytes.

Notably, several recent studies reported highly ordered interfacial adsorbates [96–98] that can promote interfacial reconstruction to form interfacial superstructures, even at general, incoherent boundaries (Fig. 5(b)) [97]. These recent observations made in the Bi-doped Ni and similar systems using aberration-corrected scanning transmission microscopy (AC STEM) [96,97] call for further investigation of several open questions: Can such ordered interfacial adsorbates and the accompanying interfacial reconstruction also exist and play important roles in battery interfaces? What are the characteristics of the 2D interfacial phases in metallic electrodes, such as lithium (Li) or tin (Sn) anodes, including their interfaces with solid or liquid electrolytes?

Thermodynamic, there is a distinction between 2D interfacial phases (complexions) and thin layers of 3D bulk phases precipitated at interfaces. However, this difference may not be easily differentiated in many practical interfaces in battery systems, for example, in the solid-electrolyte interphases (SEIs) where the two can often co-exist and be mixed. Moreover, 2D interfacial phases or complexions can often serve as the "precursors" to precipitate (thin layers of) 3D bulk phases.

4. Spontaneous formation of 2D surface phases to improve battery electrodes

A series of studies [22,24,25,28,34,53–56] suggested that the formation of nanoscale SAFs can improve the performance of Li-ion battery materials. In 2009, two interesting reports appeared. On the one hand, Tang et al. used a phase-field model to suggest that nanoscale SAFs can form in $LiMPO_4$ (M = Fe, Mn, Co, Ni) olivines to affect their phase transformation during electrochemical cycling [99]. On the other hand, Kang and Ceder reported that the formation of a glassy $Li_4P_2O_7$-like "fast ion-conducting surface phase" (<5 nm) in "off-stoichiometric" $LiFePO_4$ can help to achieve ultrafast discharging [22]. This latter report [22] led to a debate [100,101]. A technical comment [100] suggested: "There is no reason to believe that $Li_4P_2O_7$ impurity will coat the particles. Instead, impurities usually form nanoparticles that stick on the surfaces." The follow-up study by Kayyar et al. [34] showed that such coatings can form. That study [34] further demonstrated that such $Li_4P_2O_7$-based SAFs exhibit an self-selecting or "equilibrium" thickness that is independent of kinetic factors, but reversibly depends on the equilibrium temperature

(akin to those V_2O_5-based SAFs on TiO_2 shown in Fig. 1 [29,44]). In 2012, Chong et al. carefully re-examined Kang and Ceder's material and benchmarked it with carbon-coated $LiFePO_4$; their study confirmed the formation of $Li_4P_2O_7$-based "fast ion-conducting surface phase" and its effects on improving the rate performance (on a par with carbon-coated $LiFePO_4$) [28].

Kayyar et al.'s study [34] also revealed the simultaneous formation of SAFs and IGFs in sintered $LiFePO_4$ cathode (Fig. 4(a)), which suggests the possible role of IGFs in improving the rate capability. Because these cathode powders were annealed at ~600 °C to form secondary particles with sintering necks, IGFs could form along with SAFs to provide fast ion transport pathways together. This configuration was also confirmed by Chong et al. subsequently [28].

A further study systematically examined that the spontaneous formation of nanoscale Li_3PO_4-based SAFs in two proof-of-concept systems, $LiNi_{0.5}Mn_{1.5}O_4$ (Fig. 3(a)) and $LiCoO_2$ (Fig. 3(b)), their impacts on the improving the battery cycling stability and rate capability, and the underlying mechanisms [24]. These Li_3PO_4-based SAFs formed spontaneously upon facile "mixing and annealing" with self-regulating or "equilibrium" thicknesses of ~2.5 nm and ~2.9 nm, respectively, on $LiNi_{0.5}Mn_{1.5}O_4$ and $LiCoO_2$, respectively. The equilibrium thickness is independent of the amount of the Li_3PO_4 added, as shown in Fig. 3(b) (i.e., addition of an excess amount of SAF-forming additives would not result in thicker SAFs but formed a secondary phase). For example, adding 2 vol % vs. 5 vol % Li_3PO_4 to $LiCoO_2$ produced 2.90 ± 2.17 nm vs. 2.97 ± 2.00 nm thick SAFs after equilibration at 600 °C (Fig. 3(b)), where thicknesses are almost identical within the measurement errors.

The spontaneous formation of nanometer-thick Li_3PO_4-based SAFs improved the cycling stability and rate capability of $LiNi_{0.5}Mn_{1.5}O_4$ and $LiCoO_2$. For example, at a high discharge rate of 25C, these SAFs improve the discharge capacity by ~40% for $LiMn_{1.5}Ni_{0.5}O_4$ and by ~130% for $LiCoO_2$, respectively. Furthermore, these SAFs improve the cycling stability and reduce capacity fading. For example, in an accelerated test conducted at an elevated temperature of 55 °C, Li_3PO_4-based SAFs can help to maintain ~90 mAh/g discharge capacity of the high-voltage material $LiNi_{0.5}Mn_{1.5}O_4$ after 350 cycles at a charge/discharge rate of 1C. Further mechanistic studies [24] suggest that these SAFs (*i*) increase the rate capabilities by reducing the interfacial charge transfer resistance and (*ii*) improve the cycling stability by suppressing the growth of the solid-electrolyte interphase or SEI.

This facile and scalable surface modification method with spontaneous formation of 2D surface phases can be utilized to improve a broad range of other battery materials. Essentially, we let thermodynamics make nanoscale coatings for us, since SAFs or other 2D surface phases form at thermodynamic equilibria. In a recent study, the formation of nanoscale Li_3PO_4-based SAFs was also shown to significantly improve the capability of $Li_{1.33}Ni_{0.3}Mn_{0.57}O_4$ Li-excess layered oxide (Fig. 3(c)) to maintain a high capacity of 201 mAh g^{-1} after 60 cycles at 55 °C with a rate of 1 C [25].

Other types of 2D surfaces can also form in battery cathode and anode materials to improve their performance properties. Three examples beyond nanoscale SAFs are discussed below.

First, the spontaneous formation of a WO_3-rich 2D surface phase on $Li_{1.33}Ni_{0.3}Mn_{0.57}O_4$ Li-excess layered oxide cathode particles upon mixing (adding 1% WO_3) and annealing (at 800 °C) improved the discharge capacities at all rates (Fig. 3(d)) [27]. Here, this WO_3-rich surface phase is characterized by a decreased surface Ni/Mn ratio (to change the Mn-rich surface of the undoped $Li_{1.33}Ni_{0.3}Mn_{0.57}O_4$ to a Ni-rich surface, along with surface W segregation; see Fig. 3(d)) and different surface valence states (i.e., surface reduction of tungsten from W^{6+} in the bulk to W^{5+} at the surface, along with a surface enrichment of Mn^{3+} cations vs. the dominating Mn^{4+} inside the bulk phase) according to X-ray photoelectron spectroscopy (XPS). HRTEM further revealed some levels of surface disordering (but in absence of discrete nanoscale SAFs; much less disordered than the Li_3PO_4-based SAFs on $Li_{1.33}Ni_{0.3}Mn_{0.57}O_4$ shown in Fig. 3(c)) [27]. Nonetheless, this thermodynamically-preferred surface structure represents a 2D surface phase; its spontaneous formation increased the discharge capacities (e.g., by ~13% at C/20 and by ~200% at 40C; see Fig. 3(d)) and improved the cycling stability [27].

Second, surface nitridation of the TiO_2 anode materials via annealing in flowing NH_3 can lead to the formation of a titanium oxynitride (TiO_xN_y) based surface phase to increase the rate capability by increasing the surface electronic conductivity (Fig. 3(e)) [26]. In this case, XPS revealed the formation of a TiO_xN_y-based surface phase. Similar to the prior case, HRTEM only revealed low levels of surface disordering, which increased a bit at higher equilibration temperatures. However, discrete nanoscale SAFs did not form even at high temperatures. Interestingly, nitridation at a low temperature of 450 °C led to the formation of a thinner and less-disordered TiO_xN_y-based surface phase that enhance electronic conductivity (without blocking lithium transport), achieving a capacity of ~55 mAh/g at a high discharging rate 25C [26]; this capacity (of ~55 mAh/g at 25C) is more than double of that of the controlled specimens annealed in dry air under the same heat treatment condition [26], and it is better than those reported in all prior studies [102–107]. In this case, a more disordered surface phase formed at a higher temperature, which might block the lithium transport, resulted in a lower capacity. In general, this work suggested another facile method to improve the performance of battery materials via thermal treatments in controlled atmospheres to form 2D surface phases spontaneously.

Third, the formation of a WO_3-rich 2D surface phase on $LiNi_{0.5}Mn_{1.5}O_4$ changed the Wulff shape of the cathode particles, which subsequently increased the rate capability by increasing the fraction of fast-charging {110} facets (Fig. 3(f)) [30]. In this study [30], a careful analysis using an Auger electron nanoprobe identified the anisotropic surface segregation. The preferential surface segregation of W cations at the {110} facets decreased its relative surface energy according to Gibbs adsorption theory, which subsequently increased the fraction of such facets according to the Wulff theory. Since the {110} facets have more open channels for fast lithium ion diffusion, increasing its surface area/fraction improved the rate performance, *e.g.*, by ~5X at a high rate of 25C. In addition, the surface segregation and partial reduction of W cations, where were revealed the XPS depth profiling, might also inhibit the formation of Mn^{3+} on the surfaces to stabilize the cathode-electrolyte interphase at high charging voltages to improve cycling stability. This work suggested yet another route (different mechanism) to utilize anisotropic surface phase formation to thermodynamically control the particle morphology, along with controlling surface properties, to improve the electrochemical performance.

All the cases discussed above collectively exemplify an opportunity of utilizing spontaneously-formed 2D surface phases as scalable and cost-effective methods to improve battery performances via using interfacial thermodynamics (beyond the traditional ALD or other similar coating methods where the thickness of the interfacial coating is controlled by kinetic or processing parameters such as the number of ALD cycles or the deposition time and the concentration of the precursor).

5. Tailoring the ionic conductivity of solid electrolytes

A series of recent modeling and experimental studies suggested that the amorphous-like (and potentially other types of) interfacial phases can significantly affect the ion conductivity (either beneficially or detrimentally). Here, it is useful to first discuss interfacial ionic transport more broadly, since the relevant studies on lithium and sodium conductors are still rare to date. However, we believe that there are significant future opportunities for using 2D interfacial phases to engineer the ionic conductivity (as well as the processing as discussed subsequently in the next section) of the solid electrolytes used in solid-state batteries.

In 2005, Li and Garofalini used molecular dynamics simulations to suggest that nanoscale IGFs can serve as fast Li ion transport pathway in V_2O_5 [108]. Recent studies showed that phosphate-based SAFs and IGFs can often form together in annealed battery cathode particles to provide a fast Li^+ conduction pathway (Fig. 4(a)), as we have discussed previously

[22,28,34]. In 2008, De Jonghe and co-workers showed that the formation of 1–4 nm thick, impurity-based IGFs in lanthanum phosphate solid electrolytes increased the proton conductivity by more than an order of magnitude (Fig. 4(b)) [109]. A more recent study further showed that the oxygen-ion conductivities of $La_2Mo_2O_9$ nanowires can be increased by > 1000X via fast conduction in SAFs strained on the curved crystal surfaces (Fig. 4(c)), as a result of the curvatures, excess volume, and structural gradients [33].

We should further note that IGFs are not always beneficial for ionic conduction. For example, it is well known that the formation of siliceous IGFs in acceptor-doped ZrO_2 and CeO_2 oxygen-ion conductors block the oxygen ion conduction [110] and Kim et al. recently reported Ce-deficient amorphous-like IGFs in $CeZrO_3$ retarded the proton conduction [111]. We hypothesize that certain (*e.g.*, phosphate-based) liquid-like IGFs can be beneficial for Li^+ or Na^+ conduction while others may be detrimental. For oxygen ion conductors, empirical methods have been developed to reduce GB resistance via co-doping (reducing the chemical potential of SiO_2) or heat treatments (changing the equilibrium temperature) to destabilize the detrimental, silicate-based IGFs [36,110,111]. We propose that similar strategies can also be used to remove the detrimental interfacial phases, or promote the formation of beneficial interfacial phases, in various Li^+ and Na^+ solid electrolytes for applications in solid-state batteries in future studies.

In general, it is important to consider the doping effects not only on bulk phases, but also on interfaces (including grain and phase boundaries) and secondary phases at the same time, in order to optimize solid electrolytes. Using $Na_{3+x}Zr_2Si_{2+x}P_{1-x}O_{12}$ NASICON sodium ion conductor as an example, a recent work has suggested that the prior beliefs of doping effects on the bulk conductivity may be incorrect or at least incomplete [112]. That study [112] showed that Mg and Ni doping affected conductivity of $Na_{3+x}Zr_2Si_{2+x}P_{1-x}O_{12}$ mostly through increasing the "grain boundary conductivity" [112]. On the one hand, Mg and Ni doping only increased the bulk conductivity moderately via changing the Si:P ratio and stabilizing the high-conducting rhombohedral phase. On the other hand, Mg and Ni doping increased the apparent "grain boundary conductivity" substantially [112]. Here, one of the possible mechanisms is that Mg and Ni doping led to the formation a conducting Mg-doped γ-Na_3PO_4 secondary phase to increase the effective "grain boundary" conductivity [112]. Moreover, it is highly likely that the formation of 2D interfacial phases also played an important role here to improve the (true) grain boundary conductivity more directly; unfortunately, NASICON materials are too sensitive to the electron beam irradiation to allow HRTEM characterization of the grain boundary structures at the atomic scale to confirm this hypothesis.

For solid electrolytes, the formation and transformation of 2D interfacial phases can markedly change: (*i*) the space charges in the abutting crystals by changing the net charge accumulation at the interfacial core and (*ii*) the ion mobility along the interface by inducing interfacial structural or chemical disorder [36]. Both can have significant (positive or negative) impacts on the ionic conduction, which have not been fully recognized and explored in prior studies. Fig. 6(a) illustrates a case where the formation of TiO_{2-x}-like 2D interfacial phases (with partial reduction of Ti^{4+} to Ti^{3+} and deformation of Ti–O polyhedral) block ionic transport [113]; we have interpreted this as a generalized case of grain boundary prewetting [36].

In summary, an emerging opportunity of interfacial engineering is represented by investigating the previously-recognized roles of 2D interfacial phases and subsequently using them to tailor solid electrolytes by either remediating detrimental effects or utilizing beneficial effects [36]. In-depth discussion of interfacial engineering of solid electrolytes, particularly the opportunity of using the spontaneously-formed 2D interfacial phases to tune the ionic conductivity as well as related concepts, theories and strategies, can be found in a recent focused review [36] (and therefore not repeated here in details for brevity).

6. Sintering of solid electrolytes and solid-state batteries: A potential new opportunity

Many solid electrolytes (as well as solid-state battery systems) are difficult to sinter. Utilizing 2D interfacial phases provides a potentially new opportunity to improve the sintering processing, e.g., to reduce sintering temperatures, while controlling the microstructural development and interfacial properties at the same time to improve final properties. For example, low-temperature sintering can not only provide energy and cost savings but also minimize the technological issues related to selective volatilization of certain species (e.g., Li). It may also enable the co-sintering of electrolytes and electrodes in solid-state batteries in certain cases.

A comprehensive discussion on the controlling sintering via utilizing 2D interfacial phases is beyond the scope of this short review, but a couple of useful concepts are briefly discussed here. First, while the so-called "liquid-phase sintering" is well understood [114], it has been known since the 1950s that the addition of minor sintering aids can significantly accelerate the sintering rates well below the bulk solidus/eutectic temperatures, where bulk liquids are not yet stable. The origin of this so-called "sold-state activated sintering" has puzzled the materials community for decades. More recently, a series of studies demonstrated that nanometer-thick, sintering-aid-based, liquid-like IGFs can be stabilized at grain boundaries well below the bulk solidus lines; moreover, these studies used the enhanced mass transport in these premelting like IGFs to explain the mysterious "solid-state" activated sintering [46,57,59,85,88,94,115,116]. This mechanism provides a potential opportunity for low-temperature sintering of solid electrolytes and solid-state battery systems, which have not yet been carefully explored (particularly at the fundamental mechanism levels). Second, we should recognize that the formation of 2D interfacial phases can affect not only the fabrication processing (e.g., enabling low-temperature sintering) but also the microstructures and final material properties (e.g., ionic conductivity). Here, a new opportunity is represented by the use of 2D interfacial phases to simultaneously increase the grain boundary mass

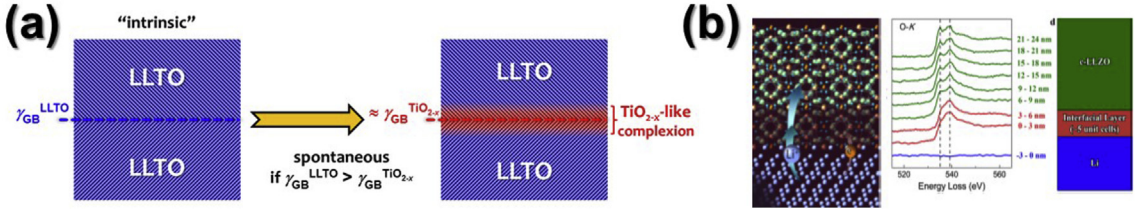

Fig. 6. Two cases of detrimental vs. beneficial 2D interfacial phases formed in solid-state battery systems. **(a)** Schematic illustration of a possible thermodynamic origin of the resistive TiO_{2-x}-like grain boundaries in LLTO observed by Ma et al. at ONRL [113], which can be explained as a generalized case of grain boundary prewetting [36]. **(b)** A most recent study at the ORNL suggested that the unusual stability of cubic LLZO-Li interfaces is related to the formation of a nanoscale tetragonal-like LLZO interfacial phase; this beneficial interfacial phase may offer interfacial stability (with its self-limiting thickness, if it is indeed a thermodynamically stable 2D interfacial phase) and perhaps some self-healing ability (with its spontaneous formation) [124]. This figure is replotted by adapting and combining original figures reported in Refs. [36,124] with permission.

transport (sintering) via inducing interfacial disordering and tailor grain boundary ion transport via tuning space charges and/or ionic mobilities.

Fundamental research is needed to enable the development of predictive models for selecting the sintering aids and designing the sintering protocols to utilize the 2D interfacial phases and their transformations to simultaneously reduce sintering temperatures and improve the final properties of solid electrolytes, beyond Edisonian trials-and-errors approach.

In this regard, an ongoing potentially-transformative research is represented by the development of grain boundray "phase" diagrams as a new materials science tool. Along this line, Luo's group extended bulk CALPHAD (calculation of phase diagrams) methods to grain boundaries to construct "grain boundary λ diagrams" to predict the thermodynamic tendency for average general grain boundaries to disorder at high temperatures. These computed grain boundary λ diagrams have been validated experimentally [57,58,85,94,95,117], and they have been used to forecast the sintering temperatures and trends [85,88,94,116,118–120]. Recent studies further computed more rigorous grain boundary "phase" diagrams with well-defined (first-order) transformation lines and critical points via using an Ising type statistical model [121] and atomistic simulations [122,123] To date, however, most of these studies have been conducted for similar metallic alloys [122] and Si–Au [123]; only one recent study first computed a grain boundary λ diagram for a simple oxide system (TiO_2–CuO) [120]. Thus, further research should be conducted to extend the successes to more complex solid electrolyte systems. If successful, such grain boundray "phase" diagrams can be used to guide the selection of materials processing recipes to utilize the formation and transformation of the most advantageous 2D interfacial phases to (1) reduce the sintering temperatures, (2) control the microstructural development, and (3) improve the interfacial properties (e.g., ionic conductivity).

7. Controlling the interfacial stability

Fig. 6(b) shows a case where the unusual stability of the interface between cubic garnet $Li_7La_3Zr_2O_{12}$ (c-LLZO) electrolyte and Li metal electrode in a solid-state battery was explained from the formation of a nanoscale tetragonal-like LLZO (t-LLZO) interfacial phase [124]. We propose that this nanoscale t-LLZO layer may be considered as an interface-stabilized 2D phase (that can be interpreted as a generalized case of prewetting). Here, the atomic structural difference between the bulk c-LLZO and interfacial t-LLZO was subtle, but the differences in electronic structures were clearly evident [124]. This case is somewhat similar to a prior observation of the formation of ~2-nm-thick reduced VO-like interfacial layers at both the VO_2–Si interface and the free surface of VO_2 (with interfacial valence changes), which was also explained as a generalized case of prewetting [125]. In this case, a coherent interface between the c-LLZO phase can help to stabilize the nanoscale t-LLZO-like interphase, which can also generate a strain energy term (in addition to the volumetric free-energy penalty for forming this t-LLZO-like layer) to limit its unrestricted thickening. If this is indeed a true 2D interfacial phase, this t-LLZO-like interphase should have formed spontaneously and conformably at the interface of c-LLZO and Li metal with self-limiting (equilibrium) thickness (akin to those IGFs). If so, this self-limiting thickness (of ~6 nm) might be the underlying reason to prevent further reactions and cause little increase in ionic resistance. Consequently, this t-LLZO-like 2D interfacial phase could offer interfacial stability (with its self-limiting thickness) and perhaps some self-healing ability (with its spontaneous formation). However, we should note that it is rather difficult to differentiate a true 2D interfacial phase (or complexion) with a thermodynamically-determined thickness from a kinetically-controlled thin layer of 3D bulk phase (both for this specific case and more generally in other SEIs), and they can often be mixed. Further in-depth characterization and fundamental studies should be conducted to draw a more solid conclusion (case by case).

In general, we propose a future opportunity to stabilize electrolyte-electrode interfaces via spontaneously-formed 2D interfacial phases (similar to those kinetically-controlled ALD coatings [8], but we let thermodynamics make them for us). As we have discussed in §4, the spontaneously-formed nanoscale SAFs can improve the cycling stability via suppressing the growth of SEI layers (Fig. 3) in liquid electrolytes [24]. Similar surface amorphous layers (albeit probably not in a full thermodynamic equilibrium) have been utilized to enhance the morphological stability of nanowires at high temperatures [126] and analogous interfacial phases have been utilized to improve the temperature-stability of nanoalloys against coarsening [127,128]. Here, we propose the possibility of stabilizing electrochemical interfaces, particularly the solid electrolyte-electrode interfaces in solid-state batteries, with 2D interfacial phases via both (1) enhancing the morphological stability (thru either reducing the thermodynamic driving force or providing the kinetic impediments) and (2) suppressing detrimental interfacial reactions and associated impedance. This innovative interfacial engineering approach has not been explored, but it represents a substantial future opportunity for stabilizing the electrolyte-electrode interfaces in both solid-state and other types of batteries.

It should be further noted that the 2D interfacial phases and thin layers of 3D bulk phases, which are rigorously different in thermodynamics, may not be easily differentiated in the SEIs of many practical systems including solid-state batteries, where they can often co-exist. The 2D interfacial phases can also serve as the "precursors" to grow into 3D bulk phases. Practically, we do not need to limit ourselves to either case, and many successful interfacial engineering approaches used today are indeed based on thin layers of 3D bulk phases. Yet, the possible existence of thermodynamically stable 2D interfacial phases or complexions offers some unique advantages, e.g., they can exhibit self-limiting or "equilibrium" thickness when they truly are 2D interfacial phases.

8. Concluding remarks

A new and potentially-transformative opportunity has emerged to utilize the equilibrium formation of 2D interfacial phases, also known as "complexions," to tailor battery materials, including electrodes, solid electrolytes, and solid-state batteries. For example, spontaneous formation of dopant-based SAFs with self-selecting thickness on the order of 1 nm and other (thinner and more ordered) 2D surface phases, which formed via facile "mixing and annealing" processes, have been utilized to improve the rate capability and cycling stability of various electrode materials. Moreover, their grain-boundary counterparts, equilibrium-thickness IGFs and other similar 2D interfacial phases have also been found in solid electrolytes or solid electrolyte-electrode interfaces. A variety of other complexions, including generalized prewetting and premelting as well as various ordered adsorbates (e.g., the series of discrete Dillon-Harmer complexions [19,21]), can also form on electrode surfaces/interfaces, grain boundaries in solid electrolytes, and solid electrolyte-electrode interfaces. Such 2D interfacial phases can control the processing, ionic conductivity, and the stability of electrochemical interfaces. A further potentially transformative idea is to utilize 2D interfacial phases to achieve superior properties unattainable by 3D bulk phases.

Specifically, various opportunities exist to use such 2D interfacial phases to improve the processing (e.g., lowering the sintering temperatures of the otherwise difficult-to-sinter solid electrolytes or solid-state battery systems) and performance properties of solid electrolytes (e.g., reducing the high grain boundray resistance) and solid-state battery systems (e.g., stabilizing the electrolyte-electrode interfaces). Here, the fundamental understandings and predictive models, which have been partially established only for simpler material systems to date, must be developed for more complex interfaces in solid electrolytes, solid-state batteries, and other advanced energy systems to enable the proposed transformative research.

Acknowledgement

This work was supported as part of the Center for Synthetic Control Across Length-scales for Advancing Rechargeables (SCALAR), an Energy Frontier Research Center funded by the United States Department of Energy, Office of Science, Basic Energy Sciences under Award # DE-SC0019381.

References

[1] X. Meng, X.-Q. Yang, X. Sun, Emerging applications of atomic layer deposition for lithium-ion battery studies, Adv. Mater. 24 (2012) 3589–3615, https://doi.org/10.1002/adma.201200397.
[2] L.A. Riley, et al., Electrochemical effects of ALD surface modification on combustion synthesized LiNi1/3Mn1/3Co1/3O2 as a layered-cathode material, J. Power Sources 196 (2011) 3317–3324, https://doi.org/10.1016/j.jpowsour.2010.11.124.
[3] Y.S. Jung, et al., Enhanced stability of LiCoO2 cathodes in lithium-ion batteries using surface modification by atomic layer deposition, J. Electrochem. Soc. 157 (2010) A75–A81, https://doi.org/10.1149/1.3258274.
[4] I.D. Scott, et al., Ultrathin coatings on nano-LiCoO2 for Li-ion vehicular applications, Nano Lett. 11 (2011) 414–418, https://doi.org/10.1021/nl1030198.
[5] D. Guan, J.A. Jeevarajan, Y. Wang, Enhanced cycleability of LiMn2O4 cathodes by atomic layer deposition of nanosized-thin Al2O3 coatings, Nanoscale 3 (2011) 1465–1469, https://doi.org/10.1039/c0nr00939c.
[6] J. Zhao, Y. Wang, Ultrathin surface coatings for improved electrochemical performance of lithium ion battery electrodes at elevated temperature, J. Phys. Chem. C 116 (2012) 11867–11876, https://doi.org/10.1021/jp3010629.
[7] X. Li, et al., Atomic layer deposition of solid-state electrolyte coated cathode materials with superior high-voltage cycling behavior for lithium ion battery application, Energy Environ. Sci. 7 (2014) 768–778.
[8] X. Han, et al., Negating interfacial impedance in garnet-based solid-state Li metal batteries, Nat. Mater. 16 (2017) 572.
[9] Y. Cao, X. Meng, J.W. Elam, Atomic layer deposition of LixAlyS solid-state electrolytes for stabilizing lithium-metal anodes, ChemElectroChem 3 (2016) 858–863.
[10] Y.S. Jung, et al., Unexpected improved performance of ALD coated LiCoO2/graphite Li-ion batteries, Adv. Energy Mater. 3 (2013) 213–219.
[11] J. Liu, X. Sun, Elegant design of electrode and electrode/electrolyte interface in lithium-ion batteries by atomic layer deposition, Nanotechnology 26 (2014), 024001.
[12] A.J. Pearse, et al., Nanoscale solid state batteries enabled by thermal atomic layer deposition of a lithium polyphosphazene solid state electrolyte, Chem. Mater. 29 (2017) 3740–3753.
[13] A. Kohandehghan, et al., Silicon nanowire lithium-ion battery anodes with ALD deposited TiN coatings demonstrate a major improvement in cycling performance, J. Mater. Chem. 1 (2013) 12850–12861.
[14] K.B. Gandrud, A. Pettersen, O. Nilsen, H. Fjellvåg, High-performing iron phosphate for enhanced lithium ion solid state batteries as grown by atomic layer deposition, J. Mater. Chem. 1 (2013) 9054–9059.
[15] J.F. Oudenhoven, L. Baggetto, P.H. Notten, All-solid-state lithium-ion microbatteries: a review of various three-dimensional concepts, Advanced Energy Materials 1 (2011) 10–33.
[16] Put, B. et al. in Meeting Abstracts. vols. 347–347 (The Electrochemical Society)..
[17] Z. Chen, Y. Qin, K. Amine, Y.-K. Sun, Role of surface coating on cathode materials for lithium-ion batteries, J. Mater. Chem. 20 (2010) 7606–7612.
[18] M. Tang, W.C. Carter, R.M. Cannon, Diffuse interface model for structural transitions of grain boundaries, Phys. Rev. B 73 (2006), 024102.
[19] P.R. Cantwell, et al., Grain boundary complexions, Acta Mater. 62 (2014) 1–48. https://doi.org/10.1016/j.actamat.2013.07.037.
[20] W.D. Kaplan, D. Chatain, P. Wynblatt, W.C. Carter, A review of wetting versus adsorption, complexions, and related phenomena: the rosetta stone of wetting, J. Mater. Sci. 48 (2013) 5681–5717.
[21] S.J. Dillon, M. Tang, W.C. Carter, M.P. Harmer, Complexion: A new concept for kinetic engineering in materials science, Acta Mater. 55 (2007) 6208–6218.
[22] B. Kang, G. Ceder, Battery materials for ultrafast charging and discharging, Nature 458 (2009) 190–193.
[23] A. Kayyar, H. Qian, Luo, J. Surface adsorption and disordering in LiFePO4 based battery cathodes, Appl. Phys. Lett. 95 (2009) 221905.
[24] J. Huang, J.A. Luo, Facile and generic method to improve cathode materials for lithium-ion batteries via utilizing nanoscale surface amorphous films of self-regulating thickness, Phys. Chem. Chem. Phys. 16 (2014) 7786–7798.
[25] H. Liu, et al., Communication—enhancing the electrochemical performance of lithium-excess layered oxide Li1. 13Ni0. 3Mn0. 57O2 via a facile nanoscale surface modification, J. Electrochem. Soc. 163 (2016) A971–A973.
[26] M. Samiee, J. Luo, A facile nitridation method to improve the rate capability of TiO 2 for lithium-ion batteries, J. Power Sources 245 (2014) 594–598.
[27] J. Huang, H. Liu, T. Hu, Y.S. Meng, Luo, J. Enhancing the electrochemical performance of Li-rich layered oxide Li 1.13 Ni 0.3 Mn 0.57 O 2 via WO 3 doping and accompanying spontaneous surface phase formation, J. Power Sources 375 (2018) 21–28.
[28] J. Chong, et al., Towards the understanding of coatings on rate performance of LiFePO4, J. Power Sources 200 (2012) 67–76, https://doi.org/10.1016/j.jpowsour.2011.10.073.
[29] J. Luo, Y.-M. Chiang, Wetting and prewetting on ceramic surfaces, Annu. Rev. Mater. Res. 38 (2008) 227–249, https://doi.org/10.1146/annurev.matsci.38.060407.132431.
[30] J. Huang, et al., Enhancing the ion transport in LiMn1. 5Ni0. 5O4 by altering the particle Wulff shape via anisotropic surface segregation, ACS Appl. Mater. Interfaces 9 (2017) 36745–36754.
[31] D.R. Clarke, On the equilibrium thickness of intergranular glass phases in ceramic materials, J. Am. Ceram. Soc. 70 (1987) 15–22.
[32] J. Luo, Stabilization of nanoscale quasi-liquid interfacial films in inorganic materials: a review and critical assessment, Crit. Rev. Solid State Mater. Sci. 32 (2007) 67–109.
[33] W. Liu, et al., Suppressed phase transition and giant ionic conductivity in La2Mo2O9 nanowires, Nat. Commun. 6 (2015) 8354, https://doi.org/10.1038/ncomms9354.
[34] A. Kayyar, H.J. Qian, Luo, J. Surface adsorption and disordering in LiFePO4 based battery cathodes, Appl. Phys. Lett. 95 (2009) 221905, https://doi.org/10.1063/1.3270106.
[35] G. Harley, R. Yu, L.C. De Jonghe, Proton transport paths in lanthanum phosphate electrolytes, Solid State Ionics 178 (2007) 769–773, https://doi.org/10.1016/j.ssi.2007.03.011.
[36] J. Luo, Interfacial engineering of solid electrolytes, J. Materiom. 1 (2015) 22–32. https://doi.org/10.1016/j.jmat.2015.03.002.
[37] Q. Ma, et al., Scandium-substituted Na3Zr2 (SiO4) 2 (PO4) prepared by a solution-assisted solid-state reaction method as sodium-ion conductors, Chem. Mater. 28 (2016) 4821–4828.
[38] J. Rickman, Luo, J. Layering transitions at grain boundaries, Curr. Opin. Solid State Mater. Sci. 20 (2016) 225–230.
[39] J. Luo, Y.-M. Chiang, R.M. Cannon, Nanometer-thick surficial films in oxides as a case of prewetting, Langmuir 21 (2005) 7358–7365.
[40] H. Qian, Luo, J. Nanoscale surficial films and a surface transition in V 2 O 5–TiO 2-based ternary oxide systems, Acta Mater. 56 (2008) 4702–4714.
[41] J. Luo, M. Tang, R.M. Cannon, W.C. Carter, Y.-M. Chiang, Pressure-balance and diffuse-interface models for surficial amorphous films, Mater. Sci. Eng. A 422 (2006) 19–28, https://doi.org/10.1016/j.msea.2006.01.001.
[42] J. Luo, Y.-M. Chiang, Existence and stability of nanometer-thick disordered films on oxide surfaces, Acta Mater. 48 (2000) 4501–4515.
[43] J. Luo, Y.-M. Chiang, Equilibrium-thickness amorphous films on {1120} surfaces of Bi 2 O 3-doped ZnO, J. Eur. Ceram. Soc. 19 (1999) 697–701.
[44] H.J. Qian, J. Luo, Vanadia-based equilibrium-thickness amorphous films on anatase (101) surfaces, Appl. Phys. Lett. 91 (2007), https://doi.org/10.1063/1.2768315, 061909.
[45] H. Qian, Luo, J. Nanoscale surficial films and A surface transition in V2O5-TiO2-based ternary oxide systems, Acta Mater. 56 (2008) 4702–4714, https://doi.org/10.1016/j.actamat.2008.05.027.
[46] J. Luo, Stabilization of nanoscale quasi-liquid interfacial films in inorganic materials: a review and critical assessment, Crit. Rev. Solid State Mater. Sci. 32 (2007) 67–109, https://doi.org/10.1080/10408430701364388.
[47] W.D. Kaplan, Y. Kauffmann, Structural order in liquids induced by interfaces with crystals, Annu. Rev. Mater. Res. 36 (2006) 1–48.
[48] C. Li, L. Gu, J. Maier, Enhancement of the Li conductivity in LiF by introducing glass/crystal interfaces, Adv. Funct. Mater. 22 (2012) 1145–1149, https://doi.org/10.1002/adfm.201101798.
[49] A. Schirmeisen, et al., Fast interfacial ionic conduction in nanostructured glass ceramics, Phys. Rev. Lett. 98 (2007) 225901, 225901 10.1103/PhysRevLett.98.225901.
[50] D.R. Clarke, T.M. Shaw, A.P. Philipse, R.G. Horn, Possible electrical double-layer contribution to the equilibrium thickness of intergranular glass films in polycrystalline ceramics, J. Am. Ceram. Soc. 76 (1993) 1201–1204.
[51] J. Luo, Y.-M. Chiang, Equilibrium-thickness amorphous films on {11-20} surfaces of Bi_2O_3-doped ZnO, J. Eur. Ceram. Soc. 19 (1999) 697–701, https://doi.org/10.1016/S0955-2219(98)00299-4.
[52] M. Baram, D. Chatain, W.D. Kaplan, Nanometer-thick equilibrium films: the interface between thermodynmaics and atomistics, Science 332 (2011) 206–209.
[53] K. Sun, S.J. Dillon, A mechanism for the improved rate capability of cathodes by lithium phosphate surficial films, Electrochem. Commun. 13 (2011) 200–202, https://doi.org/10.1016/j.elecom.2010.12.013.
[54] X.W. Li, et al., Enhanced electrochemical properties of nano-Li3PO4 coated on the LiMn2O4 cathode material for lithium ion battery at 55 degrees C, Mater. Lett. 66 (2012) 168–171, https://doi.org/10.1016/j.matlet.2011.08.075.
[55] D. Chen, et al., Effect of Li 3 PO 4 coating of layered lithium-rich oxide on electrochemical performance, J. Power Sources 341 (2017) 147–155.
[56] Z. Wang, S. Luo, J. Ren, D. Wang, X. Qi, Enhanced electrochemical performance of Li-rich cathode Li [Li 0.2 Mn 0.54 Ni 0.13 Co 0.13] O 2 by surface modification with lithium ion conductor Li 3 PO 4, Appl. Surf. Sci. 370 (2016) 437–444.
[57] V.K. Gupta, D.H. Yoon, H.M. Meyer III, Luo, J. Thin intergranular films and solid-state activated sintering in nickel-doped tungsten, Acta Mater. 55 (2007) 3131–3142, https://doi.org/10.1016/j.actamat.2007.01.017.
[58] X. Shi, Luo, J. Grain boundary wetting and prewetting in Ni-doped Mo, Appl. Phys. Lett. 94 (2009) 251908, https://doi.org/10.1063/1.3155443.
[59] J. Luo, V. Gupta, D. Yoon, H. Meyer III, Segregation-induced grain boundary premelting in nickel-doped tungsten, Appl. Phys. Lett. 87 (2005) 231902.

[60] T. Hu, S. Yang, N. Zhou, Y. Zhang, Luo, J. Role of disordered bipolar complexions on the sulfur embrittlement of nickel general grain boundaries, Nat. Commun. 9 (2018) 2764, https://doi.org/10.1038/s41467-018-05070-2.

[61] J.D. Schuler, O.K. Donaldson, T.J. Rupert, Amorphous complexions enable a new region of high temperature stability in nanocrystalline Ni-W, Scripta Mater. 154 (2018) 49–53.

[62] R.M. Cannon, et al., Adsorption and wetting mechanisms at ceramic grain boundaries, Ceram. Trans. 118 (2000) 427–444.

[63] J.G. Dash, J.S. Wettlaufer, Classical rotational inertia of solid He-4, Phys. Rev. Lett. 94 (2005) 235301, https://doi.org/10.1103/PhysRevLett.94.235301.

[64] J.G. Dash, Surface melting, Contemp. Phys. 30 (1989) 89–100.

[65] J.F. van der Veen, B. Pluis, A.W. Denier, in: R. Vanselow, R.F. Howe (Eds.), Chemistry and Physics of Solid Surfaces, vol. 7, Berlin Springer, 1988, pp. 455–467.

[66] J.W. Cahn, Critical point wetting, J. Chem. Phys. 66 (1977) 3667–3672.

[67] M. Tang, W.C. Carter, R.M. Cannon, Grain boundary transitions in binary alloys, Phys. Rev. Lett. 97 (2006), 075502.

[68] E.W. Hart, 2-Dimensional phase transformation in grain boundaries, Scripta Metall. 2 (1968) 179–&, https://doi.org/10.1016/0036-9748(68)90222-6.

[69] E.W. Hart, in: H. Hu (Ed.), Nature and Behavior of Grain Boundaries, Plenum, 1972, pp. 155–170.

[70] M.P. Seah, Grain boundary segregation, J. Phys. F Met. Phys. 10 (1980) 1043–1064.

[71] E.D. Hondros, M.P. Seah, The theory of grain boundary segregation in terms of surface adsorption analogues, Metall. Trans. 8A (1977) 1363–1371.

[72] J.W. Cahn, Transition and phase equilibria among grain boundary structures, J. Phys. 43 (1982) C6.

[73] R. Kikuchi, J.W. Cahn, Grain boundary melting transition in a two-dimensional lattice-gas model, Phys. Rev. B 21 (1980) 1893–1897.

[74] R. Kikuchi, J.W. Cahn, Grain boundaries with impurities in a two-dimensional lattice-gas model, Phys. Rev. B 36 (1987) 418.

[75] C.M. Bishop, R.M. Cannon, W.C. Carter, A diffuse interface model of interfaces: grain boundaries in silicon nitride, Acta Mater. 53 (2005) 4755–4764.

[76] C.M. Bishop, M. Tang, R.M. Cannon, W.C. Carter, Continuum modelling and representations of interfaces and their transitions in materials, Mater. Sci. Eng. A 422 (2006) 102–114.

[77] P. Wynblatt, D. Chatain, Solid-state wetting transitions at grain boundaries, Mater. Sci. Eng. A-Struc. Mater. Prop. Microstruc. Process. 495 (2008) 119–125, https://doi.org/10.1016/j.msea.2007.09.091.

[78] P. Wynblatt, D. Chatain, Anisotropy of segregation at grain boundaries and surfaces (vol 37A, pg 2595, 2006), Metall. Mater. Trans. A-Phys. Metall. Mater. Sci. 38A (2007) 438–439, https://doi.org/10.1007/s11661-006-9039-8.

[79] P. Wynblatt, D. Chatain, Anisotropy of segregation at grain boundaries and surfaces, Metall. Mater. Trans. A-Phys. Metall. Mater. Sci. 37A (2006) 2595–2620, https://doi.org/10.1007/bf02586096.

[80] T. Frolov, M. Asta, Y. Mishin, Phase transformations at interfaces: observations from atomistic modeling, Curr. Opin. Solid State Mater. Sci. 20 (2016) 308–315. https://doi.org/10.1016/j.cossms.2016.05.003.

[81] T. Frolov, Y. Mishin, Phases, phase equilibria, and phase rules in low-dimensional systems, J. Chem. Phys. 143 (2015), https://doi.org/10.1063/1.4927414, 044706.

[82] T. Frolov, D.L. Olmsted, M. Asta, Y. Mishin, Structural phase transformations in metallic grain boundaries, Nat. Commun. 4 (2013) 1899, https://doi.org/10.1038/ncomms2919.

[83] T. Frolov, S.V. Divinski, M. Asta, Y. Mishin, Effect of interface phase transformations on diffusion and segregation in high-angle grain boundaries, Phys. Rev. Lett. 110 (2013) 255502, https://doi.org/10.1103/PhysRevLett.110.255502.

[84] Y. Mishin, W.J. Boettinger, J.A. Warren, G.B. McFadden, Thermodynamics of grain boundary premelting in alloys. I. Phase-field modeling, Acta Mater. 57 (2009) 3771–3785.

[85] J. Luo, X.M. Shi, Grain boundary disordering in binary alloys, Appl. Phys. Lett. 92 (2008) 101901, https://doi.org/10.1063/1.2892631.

[86] J. Luo, Grain boundary complexions: the interplay of premelting, prewetting, and multilayer adsorption, Appl. Phys. Lett. 95 (2009), https://doi.org/10.1063/1.3212733, 071911.

[87] J. Luo*, H. Cheng, K.M. Asl, C.J. Kiely, M.P. Harmer*, The role of a bilayer interfacial phase on liquid metal embrittlement, Science 333 (2011) 1730–1733, https://doi.org/10.1126/science.1208774.

[88] J. Luo, Developing interfacial phase diagrams for applications in activated sintering and beyond: current status and future directions, J. Am. Ceram. Soc. 95 (2012) 2358–2371, https://doi.org/10.1111/j.1551-2916.2011.05059.x.

[89] S.J. Dillon, M.P. Harmer, Multiple grain boundary transitions in ceramics: a case study of alumnia, Acta Mater. 55 (2007) 5247–5254.

[90] M.P. Harmer, Interfacial kinetic engineering: how far have we come since kingery's inaugural sosman address? J. Am. Ceram. Soc. 93 (2010) 301–317, https://doi.org/10.1111/j.1551-2916.2009.03545.x.

[91] M.P. Harmer, The phase behavior of interfaces, Science 332 (2011) 182–183.

[92] P.R. Cantwell, et al., Overview No. 152: grain boundary complexions, Acta Mater. 62 (2014) 1–48. https://doi.org/10.1016/j.actamat.2013.07.037.

[93] S. Ma, et al., A grain-boundary phase transition in Si-Au, Scripta Mater. 66 (2012) 203–206, https://doi.org/10.1016/j.scriptamat.2011.10.011.

[94] X. Shi, Luo, J. Developing grain boundary diagrams as a materials science tool: a case study of nickel-doped molybdenum, Phys. Rev. B 84 (2011), https://doi.org/10.1103/PhysRevB.84.014105, 014105.

[95] X. Shi, Luo, J. Decreasing the grain boundary diffusivity in binary alloys with increasing temperature, Phys. Rev. Lett. 105 (2010) 236102, https://doi.org/10.1103/PhysRevLett.105.236102.

[96] J. Luo, H. Cheng, K.M. Asl, C.J. Kiely, M.P. Harmer, The role of a bilayer interfacial phase on liquid metal embrittlement, Science 333 (2011) 1730–1733, https://doi.org/10.1126/science.1208774.

[97] Z. Yu, et al., Segregation-induced ordered superstructures at general grain boundaries in a nickel-bismuth alloy, Science 358 (2017) 97–101, https://doi.org/10.1126/science.aam8256.

[98] A. Kundu, K.M. Asl, J. Luo, M.P. Harmer, Identification of a bilayer grain boundary complexion in Bi-doped Cu, Scripta Mater. 68 (2013) 146–149.

[99] M. Tang, et al., Model for the particle size, overpotential, and strain dependence of phase transition pathways in storage electrodes: application to nanoscale olivines, Chem. Mater. 21 (2009) 1557–1571, https://doi.org/10.1021/cm803172s.

[100] K. Zaghib, J.B. Goodenough, A. Mauger, C. Julien, Unsupported claims of ultrafast charging of LiFePO4 Li-ion batteries, J. Power Sources 194 (2009) 1021–1023.

[101] G. Ceder, B. Kang, Response to "unsupported claims of ultrafast charging of Li-ion batteries", J. Power Sources 194 (2009) 1024–1028.

[102] H. Han, et al., Nitridated TiO2 hollow nanofibers as an anode material for high power lithium ion batteries, Energy Environ. Sci. 4 (2011) 4532–4536, https://doi.org/10.1039/c1ee02333k.

[103] J.-Y. Shin, J.H. Joo, D. Samuelis, J. Maier, Oxygen-deficient TiO2-delta nanoparticles via hydrogen reduction for high rate capability lithium batteries, Chem. Mater. 24 (2012) 543–551, https://doi.org/10.1021/cm2031009.

[104] J. Lee, et al., Direct access to mesoporous crystalline TiO2/carbon composites with large and uniform pores for use as anode materials in lithium ion batteries, Macromol. Chem. Phys. 212 (2011) 383–390, https://doi.org/10.1002/macp.201000687.

[105] S.K. Das, M. Patel, A.J. Bhattacharyya, Effect of nanostructuring and ex situ amorphous carbon coverage on the lithium storage and insertion kinetics in anatase titania, ACS Appl. Mater. Interfaces 2 (2010) 2091–2099, https://doi.org/10.1021/am1003409.

[106] P. Singh, M. Patel, A. Gupta, A.J. Bhattacharyya, M.S. Hegde, Sonochemical synthesis of Pt ion substituted TiO2 (Ti0.9Pt0.1O2): a high capacity anode material for lithium battery, J. Electrochem. Soc. 159 (2012) A1189–A1197, https://doi.org/10.1149/2.029208jes.

[107] S. Yoon, B.H. Ka, C. Lee, M. Park, S.M. Oh, Preparation of nanotube TiO2-carbon composite and its anode performance in lithium-ion batteries, Electrochem. Solid State Lett. 12 (2009) A28–A32, https://doi.org/10.1149/1.3035981.

[108] W.Q. Li, S.H. Garofalini, Molecular dynamics simulations of Li insertion in a nanocrystalline V2O5 thin film cathode, J. Electrochem. Soc. 152 (2005) A364–A369, https://doi.org/10.1149/1.1848345.

[109] G.J. Zhang, et al., Proton conduction and characterization of an La(PO3)(3)-Ca(PO3)(2) glass-cerarnic, Solid State Ionics 178 (2008) 1811–1816, https://doi.org/10.1016/j.ssi.2007.11.038.

[110] J.-H. Lee, Highly resistive intergranular phases in solid electrolytes: an overview, Monatshefte Chem. 140 (2009) 1081–1094, https://doi.org/10.1007/s00706-009-0111-0.

[111] H.-S. Kim, H.B. Bae, W. Jung, S.-Y. Chung, Manipulation of nanoscale intergranular phases for high proton conduction and decomposition tolerance in BaCeO3 polycrystals, Nano Lett. 18 (2018) 1110–1117.

[112] M. Samiee, et al., Divalent-doped Na3Zr2Si2PO12 natrium superionic conductor: improving the ionic conductivity via simultaneously optimizing the phase and chemistry of the primary and secondary phases, J. Power Sources 347 (2017) 229–237. https://doi.org/10.1016/j.jpowsour.2017.02.042.

[113] C. Ma, et al., Atomic-scale origin of the large grain-boundary resistance in perovskite Li-ion-conducting solid electrolytes, Energy Environ. Sci. 7 (2014) 1638–1642.

[114] R.M. German, Liquid Phase Sintering, Plenum Press, 1985.

[115] J. Luo, H. Wang, Y.-M. Chiang, Origin of solid state activated sintering in Bi2O3-doped ZnO, J. Am. Ceram. Soc. 82 (1999) 916, https://doi.org/10.1111/j.1151-2916.1999.tb01853.x.

[116] J. Luo, Liquid-like interface complexion: from activated sintering to grain boundary diagrams, Curr. Opin. Solid State Mater. Sci. 12 (2008) 81–88, https://doi.org/10.1016/j.cossms.2008.12.001.

[117] Gupta, V. K., Yoon, D. H., Luo, J. & Meyer III, H. M. in Ceramic Nanomaterials and Nanotechnology IV. (ed M. Z. Hu R. M. Lane, S. Lu) 159-174 (The American Ceramic Society).

[118] N. Zhou, T. Hu, Luo, J. Grain boundary complexions in multicomponent alloys: challenges and opportunities, Curr. Opin. Solid State Mater. Sci. 20 (2016) 268–277.

[119] N. Zhou, Luo, J. Developing grain boundary diagrams for multicomponent alloys, Acta Mater. 91 (2015) 202–216. https://doi.org/10.1016/j.actamat.2015.03.013.

[120] J. Nie, J.M. Chan, M. Qin, N. Zhou, J. Luo, Liquid-like grain boundary complexion and sub-eutectic activated sintering in CuO-doped TiO 2, Acta Mater. 130 (2017) 329–338.

[121] N. Zhou, Z. Yu, Y. Zhang, M.P. Harmer, Luo, J. Calculation and validation of a grain boundary complexion diagram for Bi-doped Ni, Scripta Mater. 130 (2017) 165–169. https://doi.org/10.1016/j.scriptamat.2016.11.036.

[122] S. Yang, N. Zhou, H. Zheng, S.P. Ong, Luo, J. First-order interfacial transformations with a critical point: breaking the symmetry at a symmetric tilt grain boundary, Phys. Rev. Lett. 120 (2018), 085702.

[123] C. Hu, J. Luo, First-order grain boundary transformations in Au-doped Si: hybrid Monte Carlo and molecular dynamics simulations verified by first-principles calculations, Scripta Mater. 158 (2019) 11–15.

[124] C. Ma, et al., Interfacial stability of Li metal–solid electrolyte elucidated via in situ electron microscopy, Nano Lett. 16 (2016) 7030–7036, https://doi.org/10.1021/acs.nanolett.6b03223.
[125] X. Li, et al., Discovery of nanoscale reduced surfaces and interfaces in VO2 thin films as a unique case of prewetting, Scripta Mater. 78–79 (2014) 41–44. https://doi.org/10.1016/j.scriptamat.2014.01.029.
[126] L. Yao, et al., Stabilizing nanocrystalline oxide nanofibers at elevated temperatures by coating nanoscale surface amorphous films, Nano Lett. 18 (2018) 130–136.
[127] N. Zhou, T. Hu, J. Huang, Luo, J. Stabilization of nanocrystalline alloys at high temperatures via utilizing high-entropy grain boundary complexions, Scripta Mater. 18 (2018) 130–136. https://doi.org/10.1016/j.scriptamat.2016.07.014.
[128] T. Chookajorn, H.A. Murdoch, C.A. Schuh, Design of stable nanocrystalline alloys, Science 337 (2012) 951–954, https://doi.org/10.1126/science.1224737.
[129] M. Samiee, Luo, J. Pseudocapacitive properties of two-dimensional surface vanadia phases formed spontaneously on titania, ACS Appl. Mater. Interfaces 8 (2016) 12871–12880, https://doi.org/10.1021/acsami.6b03569.
[130] S. Ma, et al., Grain boundary complexion transitions in WO 3-and CuO-doped TiO 2 bicrystals, Acta Mater. 61 (2013) 1691–1704.